Journal of The Electrochemical Society, **164** (7) F759-F767 (2017)
0013-4651/2017/164(7)/F759/9/$37.00 © The Electrochemical Society

Study of the Electrode Polarization Resistance of Cobaltites with High Ba Content as Cathode for IT-SOFC

C. Setevich,[a,b] F. Prado,[a,z] and A. Caneiro[b]

[a]*Departamento de Física, Universidad Nacional del Sur and IFISUR, 8000 Bahía Blanca, Argentina*
[b]*Centro Atómico Bariloche, Comisión Nacional de Energía Atómica, 8400, S. C. de Bariloche, Argentina*

The phase relationships and the electrochemical behavior of cobaltites with high content of Ba, such as, $La_{1-x}Ba_xCoO_{3-\delta}$ with x = 0.5, 0.7 and 1.0, $Ba_{0.5}Sr_{0.5}Co_{0.8}Fe_{0.2}O_{3-\delta}$ (BSCF) and $BaCo_{0.7}Fe_{0.2}Nb_{0.1}O_{3-\delta}$ (BCFN), were studied by XRD and impedance spectroscopy varying the electrode configurations from a single porous layer to a graded-cathode using $Ce_{0.9}Gd_{0.1}O_{1.95}$ (GDC) as electrolyte. Regardless of the electrode material, symmetrical cells with graded-cathodes displayed the lowest polarization resistance (R_p) values. The minimum R_p values were found to be 0.036 and 0.039 Ω cm^2 at 600°C, in air, for $La_{0.5}Ba_{0.5}CoO_{3-\delta}$ (LBC) and BSCF, respectively. The impedance spectra reveals mainly two processes, one at intermediate frequency (IF) in the range ($0.1 \leq f \leq 5 \times 10^3$ Hz) and another at low frequency (LF) in the range ($1 \leq f \leq 3$ Hz). The variation of the parameter *n* (obtained from the log(R_{IF}) vs. log(pO_2) plots) in relation with the electrode configuration, indicates the rate-limiting process goes from a mixture of the ion transfer at the electrode/electrolyte interface and the charge transfer at the electrode surface to a mixture between this last process and the dissociation of the oxygen molecule.

Manuscript submitted March 9, 2017; revised manuscript received May 1, 2017. Published May 9, 2017.

Fast oxygen exchange at the electrode surface, as well as a high ionic and electronic conductivities are important requirements for materials to be used as cathode material in intermediate-temperature solid oxide fuel cells (IT-SOFC).[1] These properties were initially reported for the perovskite system (La,Sr)(Fe,Co)$O_{3-\delta}$[2,3] and extensively investigated thereafter. More recently, other cobaltites with Ba replacing La or Sr such as $Ba_{0.5}Sr_{0.5}Co_{0.8}Fe_{0.2}O_{3-\delta}$ (BSCF),[4–6] $BaCo_{0.7}Fe_{0.2}Nb_{0.1}O_{3-\delta}$ (BCFN)[7] and $La_{0.5}Ba_{0.5}CoO_{3-\delta}$ (LBC)[8,9] have also shown good performance as cathode material for IT-SOFC. The large size of the Ba^{2+} cation (r_{Ba} = 1.60 Å)[10] gives place to a low migration energy for oxygen ions, and an increasing O-diffusivity compared to (La,Sr)(Co,Fe)O_3 perovskites.[11] Additionally, Ishihara et al.[12,13] explored the electrochemical response of $La_{1-x}Ba_xCoO_{3-\delta}$ with $0 \leq x \leq 1.0$ in SOFC single cells prepared with Co doped $La_{0.8}Sr_{0.2}Ga_{0.8}Mg_{0.2}O_{3-\delta}$ (LSGM) as electrolyte. The minimum cathode overpotential was obtained for the composition x = 0.6 at 600°C. On the other hand, Setevich et al.[14,15] studied the phase diagram and the electrochemical responses of the $La_{1-x}Ba_xCoO_{3-\delta}$ compounds by using complex impedance measurements with GDC as electrolyte, finding the lowest $R_p = 0.05$ Ω cm^2 value for x = 0.7. More recently, Rupp et al.[16] have reported superior properties for $La_{0.6}Ba_{0.4}CoO_{3-\delta}$ compared to $La_{0.6}Sr_{0.4}CoO_{3-\delta}$ electrodes for the oxygen reduction reaction. However, the cubic crystal structure of samples with high Ba content and Co in the B site tend to be unstable at T ≤ 900°C.[17] To resolve this problem, the addition of Fe and Nb at the B site of the perovskite Ba(Co, Fe, Nb)$O_{3-\delta}$ has been explored.[18,19] It was reported that $BaCo_{0.7}Fe_{0.2}Nb_{0.1}O_{3-\delta}$ (BCFN) exhibits good stability under reducing atmospheres,[19] high oxygen permeability flux values and good cathode performance for IT-SOFC.[18,19] In the case of the $La_{1-x}Ba_xCo_{1-y}M_yO_{3-\delta}$ compounds, the replacement of Co with Fe or Nb stabilizes the cubic perovskite, although the electrochemical performance of the electrodes is reduced.[20,21] Another issue for perovskites with high Co and Ba contents is the mismatch in the thermal expansion coefficient between them and the electrolytes, which leads to adhesion problems and delamination of the electrode accompanied by the degradation of the cell performance.[22] A commonly adopted strategy to reduce the mismatch is the use of composite materials by mixing the cobaltite and the electrolyte, which reduces the expansion coefficient of the electrode. In addition, several works have indicated that the cathodic response improves when using a composite as electrode.[5,15,23] However, if the electrolyte fraction forming the composite is large enough, the polarization resistance (R_p) and the electrical conductivity of the electrode will increase and decrease, respectively.[15,23] Another option is to use a graded-cathode, with layers that vary their composition from pure electrolyte to a pure electrode material.[14,15,24,25]

In view of the high electrochemical performance reported for cobaltites with high Ba content as cathode material for IT-SOFC,[4–9] the polarization resistance to the oxygen reduction reaction (ORR) of electrodes prepared with $La_{1-x}Ba_xCoO_{3-\delta}$ (x = 0.5, 0.7 and 1.0), BSCF and BCFN are compared and studied. Moreover, to reduce the expansion coefficient mismatch between the electrodes and the electrolyte, various configurations from a single material to a graded electrode were used for preparing symmetrical cells. For all the cases, the polarization resistance of the oxygen reduction reaction was determined by means of complex impedance measurements, as a function of temperature and oxygen partial pressure (pO_2). The contributions to the polarization resistance during the ORR were determined and the variations with T and pO_2 discussed as well as the performance of the various chemical compositions and electrode configurations.

Experimental

Samples of $La_{1-x}Ba_xCoO_{3-\delta}$ with x = 0.5, 0.7 and 1.0 and BSCF were prepared by an acetic acid-based gel route.[26] Stoichiometric amounts of La_2O_3, previously dried overnight at 1000°C, in air,$SrCO_3$, $BaCO_3$,$Fe(CH_3COO)_2$and $Co(CH_3COO)_2.4H_2O$ were dissolved in acetic acid. Together with water and small amounts of hydrogen peroxide, each mixture was refluxed at T∼80°C until a solution was obtained. Then the solvents were evaporated and a dark gel was formed. This gel was fired at 400°C for 2 h and then heat treated at 750°C for 24 h, in air. Due to Nb_2O_5 not being soluble in acetic acid, we prepared BCFN by solid state reaction (SSR). Therefore, required amounts of $BaCO_3$, Co_3O_4, Fe_2O_3 andNb_2O_5 were mixed and ground with a mortar and pestle and heat treated at 850°C in air. Subsequently, the powder was ball milled during 15 min using an agate milling media, pressed into pellets and sintered at T = 1100°C. In order to obtain the BCFN following the acetic acid gel route, we dissolved the BCFN sample obtained by SSR in acetic acid. Then the solution was evaporated and a dark gel was formed. This gel was fired at 400°C for 2 h and then heat treated at 750°C for 24 h, in air. All the samples were additionally heat treated at 800, 900, 1000 y 1100 °C for 8 h, and then cooled at a rate of 5°C/min, in air. The GDC material was synthesized using the combustion method. Stoichiometric amounts of Gd_2O_3 and $Ce(NO_3)_3$.$6H_2O$ were dissolved in acetic acid. The mixture was refluxed at T∼80°C until a clear solution was obtained. Then temperature was raised to approximately 300°C, at which the ignition of the solution started. To investigate the reactivity, mixtures of the cobaltites with GDC in 1:1 weight ratio were prepared using the material obtained by the acetic acid gel route at 750°C, and GDC supplied by Fuel Cell Materials. These mixtures were annealed at 800, 900

[z]E-mail: fernando.prado@uns.edu.ar

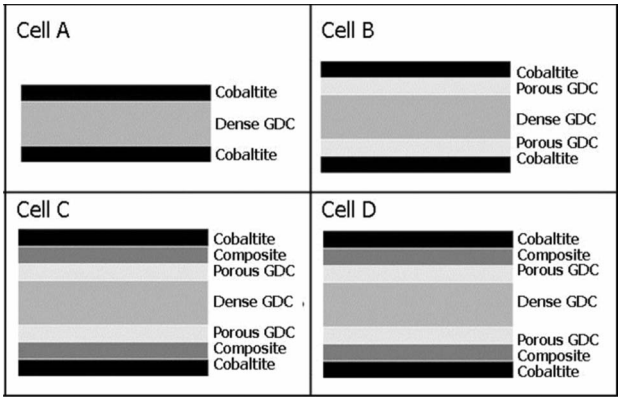

Figure 1. Scheme of the symmetrical cells electrodes used for impedance spectroscopy measurements.

and 1000°C for 8 h. The samples were analyzed by X-ray diffraction (XRD) at room temperature with a Philips PW1700 diffractometer using Cu Kα radiation and a graphite monochromator from 2θ = 10 to 80° with a counting time of 2 s per 0.02°. The crystal structures were analyzed by the Rietveld method using the FullProf Program.[27]

The polarization resistance of the electrodes was studied by EIS (Electrochemical Impedance Spectroscopy) on electrochemical cells using GDC as electrolyte and a symmetrical configuration. Commercial GDC powder from Fuel Cells Materials with a specific area of 35 m^2/g was pressed into 12.5 mm diameter disks, applying uniaxial pressure of 100 kg/cm^2, and sintered at 1350°C for 4 h, in air. After sintering, the electrolyte disks were approximately 9.8 mm in diameter and around 0.3 mm thick. The inks for electrode deposition were prepared mixing the corresponding ceramic powders with ethanol, α-terpineol, polyvinyl butyral and polyvinyl pyrrolidone in 40:30:27:2:1 ratio. For the cobaltite layers we have used the materials prepared at 750°C, while for GDC we have used GDC from Fuel Cells Materials or prepared by the combustion method. Previous to the deposition onto the electrolyte using an airbrush, the electrode material ink was stirred to assure its homogeneity. The thickness of each layer was controlled keeping constant the number of times the electrolyte was painted with the airbrush. Figure 1 shows the four electrode configurations tested:

Cell A: The electrodes consisted of a single porous layer of cobaltite sprayed onto dense GDC electrolyte.

Cell B: The electrodes consisted of a porous GDC layer sprayed onto the dense electrolyte, and then heat treated at 1300°C for 1 h, and a second porous cobaltite layer sprayed onto the porous GDC layer.

Cell C: The electrodes were prepared using three layers: a porous GDC layer similar to the one described in cell B, a layer of cobaltite + GDC in a 1:1 weight ratio and finally a porous cobaltite layer.

Cell D: The electrode configuration is similar to cell C. In this case the GDC for the porous and composite layers were prepared by the combustion method with a specific area of 70 m^2/g.

In all cases, the electrode attachment to the electrolyte was performed at around 900/950°C for 8 h, which is the temperature that yields the minimum polarization resistance at 600°C, as is described in Optimization of the heat treatment temperature for the cathode preparation section. The EIS measurements were performed varying temperature in the range 400 ≤ T ≤ 950°C by steps of 50°C and the oxygen partial pressure (pO_2) in the range $10^{-3} \leq pO_2 \leq 1$ atm by mixing Ar and O_2. The data acquisition was performed with an Autolab system PGSTAT-30 coupled to a module FRA2 in a frequency range of 1 MHz and 10^{-3} Hz. An AC signal of 20 mV was applied to the cell, under zero DC polarization. Platinum grids, slightly pressed on the porous electrodes using a Al_2O_3 tube, were used as current collectors. Impedance diagrams were analyzed using Z-view2 software.[28]

The microstructure and thickness of the porous layers and interfaces were characterized by scanning electron microscopy (SEM) using a Phillips microscope 515.

Results and Discussion

XRD characterization of $La_{1-x}Ba_xCoO_{3-\delta}$ with x = 0.5, 0.7 and 1.0, BSCF and BCFN.—The XRD characterization of the samples becomes relevant when correlating the electrochemical response and the phase relationship in the electrode, which varies with the heat-treatment temperature. In the $La_{1-x}Ba_xCoO_{3-\delta}$ samples with x = 0.5 and 0.7, prepared at 750°C, a mixture of cubic perovskite (space group $Pm\bar{3}\,m$) and a 2H hexagonal phase (space group $P6_3/mmc$)[29] was found. Figure 2a shows this result for LBC. As the heat-treatment

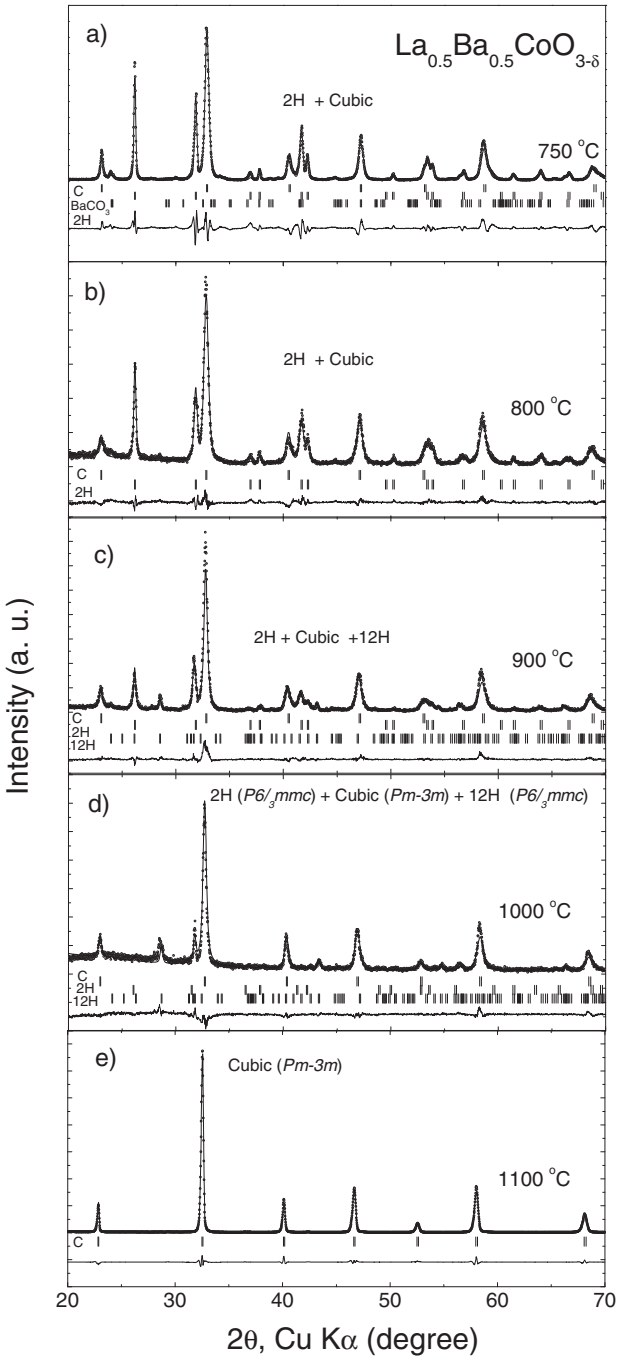

Figure 2. XRD patterns of $La_{0.5}Ba_{0.5}CoO_{3-\delta}$ sample synthesized by the acetic acid-gel method after the heat-treatment at various temperatures. a) T = 750°C for 24 h, b-e) T = 750°C for 24 h plus an extra heat-treatment for 8 h, in air, at: b) T = 800°C, c) T = 900°C, d) T = 1000°C and e) T = 1100°C. For each pattern the experimental data, calculated profile, the difference between them and the positions of the reflections allowed for the cubic, 2H and 12H phases, are included.

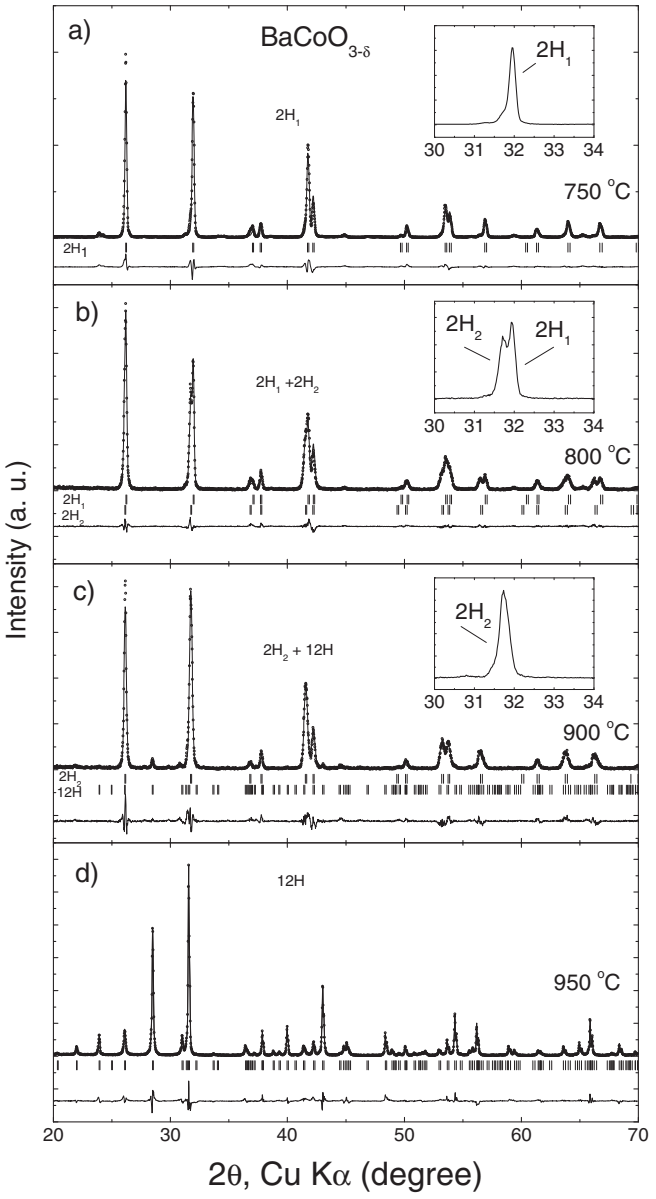

Figure 3. XRD patterns of $BaCoO_{3-\delta}$ sample synthesized by the acetic acid-gel method after the heat-treatment at various temperatures. a) T = 750°C for 24 h, b-d) T = 750°C for 24 h plus an extra heat-treatment for 8 h, in air, at: b) 800°C, c) 900°C and d) 950°C. For each pattern the experimental data, calculated profile, the difference between them and the positions of the reflections allowed for the 2H and 12H phases, are included.

temperature for electrode adhesion increased, the intensity ratio between the reflections of the cubic and the 2H hexagonal phases increased denoting the growth of the perovskite fraction. This behavior is shown in Figures 2a–2e for LBC. At 900°C (Figure 2c) the appearance of the reflection at $2\theta = 28.5^{\circ}$ indicates the formation of the 12H hexagonal phase.[30] After the heat treatments at 1100°C the 2H and 12H hexagonal phases fade away and the cubic perovskite LBC with $a = 3.880$ (1) Å is obtained. The phase relationship evolution of $La_{0.3}Ba_{0.7}CoO_{3-\delta}$ is similar to that described for LBC in Figure 2, although in this case the 2H and 12H hexagonal phase fractions are higher at T < 1100°C. For $BaCoO_{3-\delta}$ a majority 2H hexagonal phase[29] is formed at 750°C, which coexist with small amounts of CoO and $BaCO_3$, while the cubic perovskite fraction is null (see Figure 3a). After the heat-treatment at 800°C, several reflections ($2\theta = 32^{\circ}$, 41.8°, 53.5°, 56.9°) split into two peaks. Revealing the presence of two 2H hexagonal phases, the $2H_1$ phase with $a = b = 5.599$ (1) and $c =$ 4.767 (1) Å and the $2H_2$ phase with $a = b = 5.634$ (1) and $c = 4.766$ (1) Å. At 900°C (Figure 3c), only the $2H_2$ and the 12H hexagonal phase $BaCoO_{3-\delta}$ with $\delta \sim 2.60$ and lattice parameters $a = b = 5.660$ (1) and $c = 28.530$ (1) Å remains.[23] Finally, after a heat-treatment at 950°C, $BaCoO_{3-\delta}$ was found single phase with a 12H hexagonal crystal structure and lattice parameters $a = b = 5.667$ (1) and $c = 28.497$ (1) Å as is shown in Figure 3d. Variations in the crystal structure of $BaCoO_{3-\delta}$ are related to its oxygen content, which was reported to be 2H hexagonal, 12H hexagonal or cubic depending on $3-\delta = 3$, 2.6 or 2.2, respectively.[29–31] The BCFN sample heat treated at 750°C, shows the coexistence of $BaCoO_{3-\delta}$, the 2H hexagonal phase and a cubic phase of general composition $BaCo_{1-y-z}Fe_yNb_zO_{3-\delta}$. As the temperature of the heat-treatment increases, the cubic perovskite becomes the majority phase coexisting with the 2H hexagonal and the perovskite $BaFeO_{3-\delta}$ phases. Finally, the sample heat treated at 1100°C was found single phase with cubic symmetry and lattice parameter $a = 4.080$ (1) Å. For BSCF, the phase relationship evolution with the heat-treatment temperature was described in a previous work.[6]

Table I. Reactivity products after a heat-treatment at 900 and 1000°C for 8 h between the electrodes materials and GDC.

T (°C)	LBC	$La_{0.3}Ba_{0.7}CoO_{3-\delta}$	$BaCoO_{3-\delta}$	BCFN	BSCF
900	-	-	-	-	$BaCeO_3$
1000	$BaCeO_3$	$BaCeO_3$	$BaCeO_3$	$BaCeO_3$	$BaCeO_3$

Chemical reactivity with GDC.—The chemical reactivity between the cobaltites prepared at 750°C and GDC was studied between 800 and 1000°C by XRD measurements following the procedure described in Experimental section. In Table I, the heat-treatment temperature and phase formation are summarized. For $La_{1-x}Ba_xCoO_{3-\delta}$ with x = 0.5, 0.7 and 1.0 and BCFN, the appearance of $BaCeO_3$ reflections reveal chemical reactivity only at 1000°C. This temperature is lower than the value T = 1100°C obtained for $La_{1-x}Ba_xCoO_{3-\delta}$ prepared by solid state reaction,[14] possibly due to differences in the microstructure of the samples obtained by the acetate method. For BSCF, the perovskite $BaCeO_3$ shows up at 900°C as was previously reported.[6,32]

Optimization of the heat-treatment temperature for the cathode preparation.—The optimum heat-treatment temperature for the cathode preparation was determined by monitoring the polarization resistance (Rp) at 600°C after the symmetrical cell was heat treated between 750 and 950°C. Figure 4 shows the complex impedance spectra obtained at 600°C, in air, for the LBC electrode. The impedance spectra were shifted in such a way that the low frequency data points intersect the *x*-axis at $Z' = 1\ \Omega\ cm^2$. Independently of the electrode configuration and the heat-treatment temperature, the spectra consist of two arcs, a low frequency (LF) and an intermediate frequency arc (IF). As the heat-treatment temperature increases, Rp decreases as a consequence of the IF arc shrinkage, while the LF arc remains almost constant. This result clearly shows that the heat-treatment to adhere the electrode to the electrolyte, enhance the kinetic of those processes related to R_{IF}. The optimum Rp value at 600°C for cell A was obtained after the heat-treatment was performed at T = 950°C, while for cells B, C and D the optimum temperature was T = 900°C. For LBC (see Figure 4) the lowest polarization resistance value, $R_p \sim 0.036\ \Omega\ cm^2$, was obtained for cell D. The experimental data indicate Rp follow the sequence D < C < B < A. A similar behavior was observed for $La_{0.3}Ba_{0.7}CoO_{3-\delta}$, $BaCoO_{3-\delta}$, BCFN and BSCF[6] during the cathode preparation. For these cobaltites the optimum temperature was found in the temperature range $900 \leq T \leq 950$°C regardless the electrode configuration.

Microstructure.—Figure 5 shows SEM micrographs (1850 ×) of the $La_{0.3}Ba_{0.7}CoO_{3-\delta}$ electrodes cross section after impedance spectroscopy measurement for the different configurations. The thickness and uniformity of the layers forming the electrodes can be observed

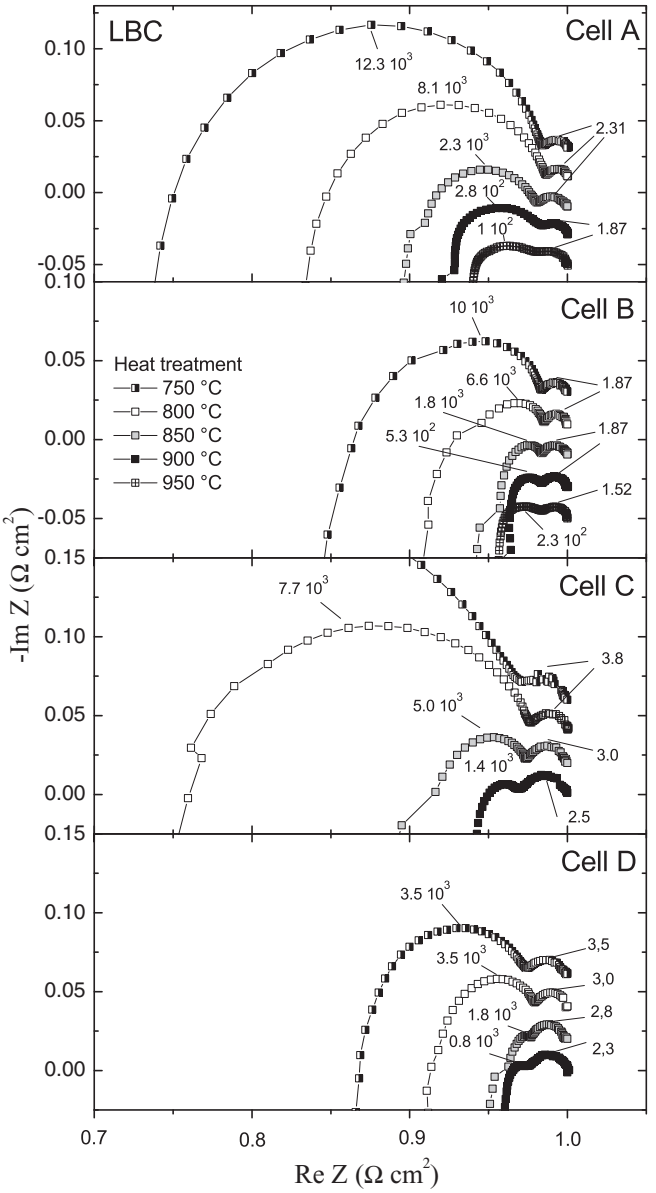

Figure 4. Complex impedance spectra for $La_{0.5}Ba_{0.5}CoO_{3-\delta}$ electrodes using cells configuratios A, B, C and D. These impedance spectra were measured at T = 600°C in ambient air after the electrode was heat treated at various temperatures between 750 and 950°C.

in Figure 5a-5d after the cells were broken to expose the cross section. No delamination was detected during impedance measurements. The particle size of the electrode material $La_{0.3}Ba_{0.7}CoO_{3-\delta}$ in the layers is in the range 1–7 μm. These values are by far larger than those observed for the particles of the sample prepared at 750°C, which presents nanometric size. As is expected, after the heat-treatment at 900°C particle size is greatly increased reducing the electrode specific area. Figure 6 compares the electrode microstructure before and after the heat-treatment for bonding the electrode to the electrolyte, which shows the ceramic grains growth. Note that the minimum R_p value was obtained after the heat-treatment at T = 900°C, that means after the ceramic grains have increased. This result shows that in addition to materials with high specific area, an optimal attachment between electrode and electrolyte is needed to low the Rp value of the electrode. Similar description for the electrode microstructure can be applied to the other materials studied in this paper. Finally, the ceramic grains

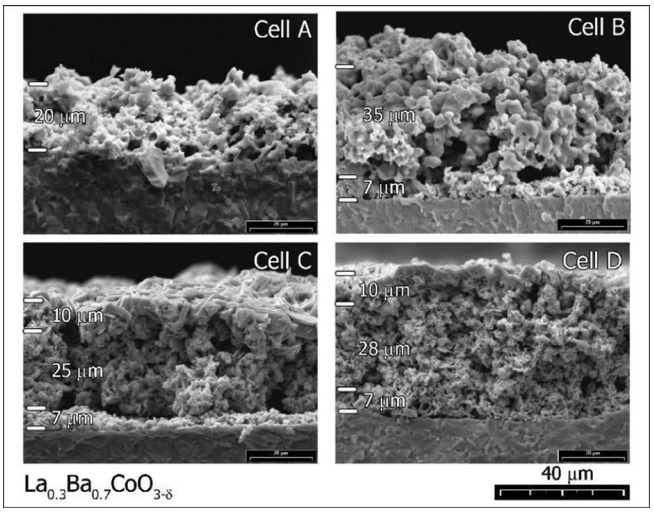

Figure 5. SEM micrographs (1850 ×)of the electrode cross section for cells A, B, C and D prepared with $La_{0.3}Ba_{0.7}CoO_{3-\delta}$.

size of GDC forming the porous layer and the composite was in the range between 0.1 and 0.5 μm.

Polarization resistance of $La_{1-x}Ba_xCoO_{3-\delta}$ with x = 0.5, 0.7 and 1.0, BSCF and BCFN electrodes.—In Figure 7 we compare Rp values obtained at 600°C for the various electrodes after optimizing the polarization resistance according the procedure described in Optimization of the heat treatment temperature for the cathode preparation section. The lowest Rp values were found for the BSCF and LBC electrodes, regardless the cell configuration. For BSCF the lowest Rp value was 0.039 Ω cm^2 using the cell C, while for LBC we obtained 0.036 Ω cm^2 using cell D. On the other hand, $BaCoO_{3-\delta}$

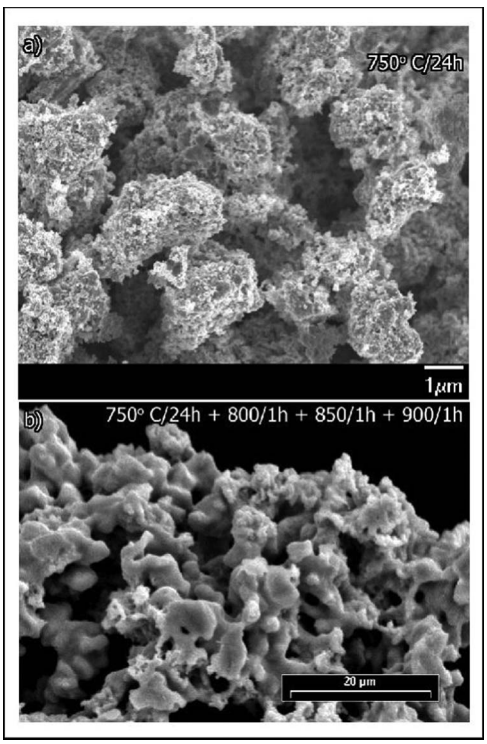

Figure 6. SEM micrographs of the microstructure of $La_{0.3}Ba_{0.7}CoO_{3-\delta}$ sample heat treated at a) 750°C, in air, for 24 h and b) 750°C / 24 h + 800°C / 1 h + 850°C/ 1h + 900°C / 1h, in air.

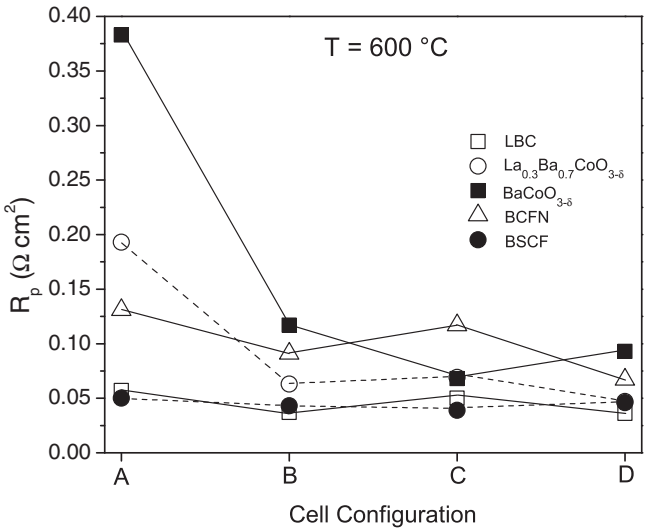

Figure 7. Polarization resistance (Rp) values measured at 600°C after determining the optimum heat-treatment temperature for electrode preparation. The electrode were prepared using LBC, $La_{0.3}Ba_{0.7}CoO_{3-\delta}$, $BaCoO_{3-\delta}$, BCFN and BSCF and symmetrical cells of the type A, B, C and D.

and $La_{0.3}Ba_{0.7}CoO_{3-\delta}$ exhibit the highest Rp values for cell A which decreases as the configuration changes toward the graded electrode of cells C or D. Systematically the lowest Rp values were obtained for cells C or D, whose electrodes were prepared using GDC with specific areas of 35 and 70 m^2/g, respectively. The variation in this parameter causes no significant difference in Rp, this is likely due to the growth of the GDC particles with temperature in the graded cathode. Figure 8 shows the Arrhenius plot of R_p for various electrodes in cells A, B, C and D. In all cases, the polarization resistance strongly decreases with increasing temperature up to T = 700°C, while for T ≥ 700°C it shows little variation. The data displayed in Figure 8 show that $BaCoO_{3-\delta}$ and BCFN exhibit the highest R_p values with the exception of $BaCoO_{3-\delta}$ in cell C. On the other hand, LBC and BSCF systematically exhibit the lowest R_p values for all the cells. As a function of temperature, small differences were observed in the behavior and magnitude of Rp. However, the lowest R_p values were obtained for graded electrodes in cells C and D. Considering the heat-treatment temperature to minimize Rp for LBC, BSCF and BCFN was found near 900°C, the majority phase

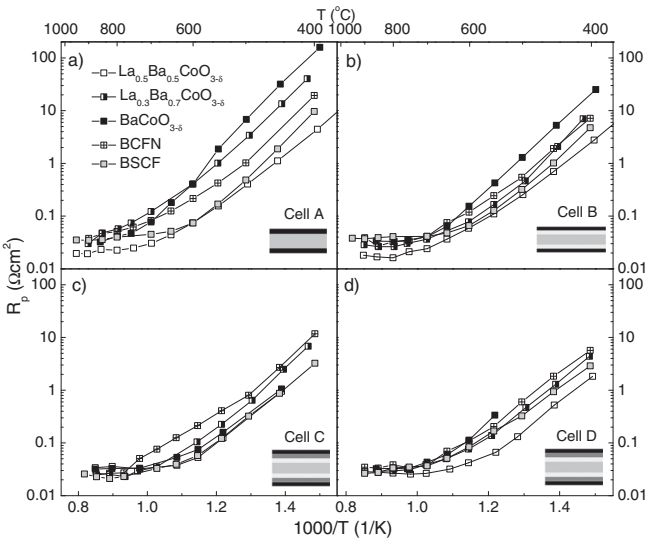

Figure 8. Arrhenius plots for the total polarization resistance Rp of electrodes prepared with LBC, $La_{0.3}Ba_{0.7}CoO_{3-\delta}$., $BaCoO_{3-\delta}$, BCFN and BSCF using the cells configurations A, B, C and D.

forming the electrodes, according to XRD data (XRD characterization of $La_{1-x}Ba_xCoO_{3-\delta}$ with x = 0.5, 0.7 and 1.0, BSCF and BCFN section) is the cubic perovskite. Thus, for cell A these materials exhibit the lowest Rp values as shown in Figure 7, while $BaCoO_{3-\delta}$, whose main phase is hexagonal, shows the highest value. However when considering cells B, C and D and their difference in the decrease of Rp the trend is not clear. In particular the electrodes prepared with $BaCoO_{3-\delta}$ have shown adherence issues to the electrolyte. Thus the use of either a porous layer of GDC or a graded cathode has improved the adhesion of the electrode to the electrolyte reducing Rp. As mentioned in Chemical reactivity with GDC section, the cobaltites react with GDC forming $BaCeO_3$ at T ≥ 900°C at the interface. The effect of the $BaCeO_3$ compound in the ORR was mentioned by Wang et al.[33] who discussed a model for a BSCF/SDC composite where chemical reaction takes place at the BSCF/SDC interface after a firing temperature of 1000°C. The authors indicated that the chemical reaction did not affect the ORR performance of the electrode also causing a good connection between the BSCF and SDC particles. The authors also indicated that because of the smaller particle size of the SDC ceramic grains in comparison to BSCF, it resulted in an increase of the effective cathode surface area. This description of the electrode microstructure is in good agreement with the morphology of the electrodes used in this work as is shown in Figure 5. However, our data show that when the heat-treatment temperature is higher than the optimal, the amount of $BaCeO_3$ and the size of the cathode ceramic grains increase and starts to affect the performance of the electrodes. Thus, the optimum heat-treatment temperature seems to regulate the amount of $BaCeO_3$ needed to obtain low Rp values.

Variation of Rp with T and pO_2.—Figure 9 shows the typical variation of the impedance spectra within the temperature range of 400 and 900°C for the various electrode materials and cells type. As an example the variation of the impedance spectra for $BaCoO_{3-\delta}$ in a cell B and LBC in a cell D are shown in Figures 9a and 9b, respectively. At high temperature, T ≥ 700°C, the LF arc with a characteristic frequency that varies between 1 and 5 Hz is the main contribution to the complex impedance. Between 500°C and 700°C a second contribution shows up at intermediate frequency (IF). For this contribution, the characteristic frequency varies between 1 and 5 × 10^3 Hz. At temperatures below 500°C a high frequency (HF) arc was detected for some electrodes with a characteristic frequency of $f > 10^4$ Hz. In addition, a very low frequency arc denominated LF* was observed at T ≤ 500°C for a couple of electrodes with a characteristic frequency below 10^{-2} Hz. In particular, the features of this contribution indicate it is not related to the LF contribution detected at T ≥ 700°C. Taking this under account, when fitting impedance data, we used the equivalent circuit displayed in Figure 10. This circuit consists of an inductance L_C in parallel with a resistor R_C representing the cables of the experimental setup in series with a R_E resistor, representing the ohmic resistance of the electrolyte, and in series with elements (Ri,CPEi) and (Rj,CPEj) representing the impedance arcs HF, IF, LF and LF*. The HF arc was included in the equivalent circuit as a minor correction of the intermediate frequency contribution in the low temperature range (T ≤ 500°C). The size of this arc is negligible and can be associated with processes which take place in the electrolyte. On the other hand, the LF* contribution was observed in the electrochemical response of BSCF in cells A and B[6] and BCFN in the cell A. It was also considered in the analysis of the data although the process associated with it is not clear. Thus, hereafter we will focalize in the analysis in the IF and LF contributions to the polarization resistance of the electrodes. Figures 11 and 12 show the Arhenius plots for R_P, R_{IF} and R_{LF} as well as the characteristic frequency and capacitance of the IF and LF contributions for the electrodes prepared with the perovskites $La_{0.3}Ba_{0.7}CoO_{3-\delta}$ and LBC, respectively. Data points for R_{IF} and R_{LF} were obtained by fitting the impedance data, like those shown in Figure 9, with the equivalent circuit displayed in Figure 10, while R_P corresponds to the sum of R_{IF} and R_{LF}. It can be seen that at low temperatures $R_P \sim R_{IF}$, while at high temperature (T ≥ 700°C) $R_p \sim R_{LF}$. Similar behavior was obtained for BCO, BCFN, and BSCF. In order

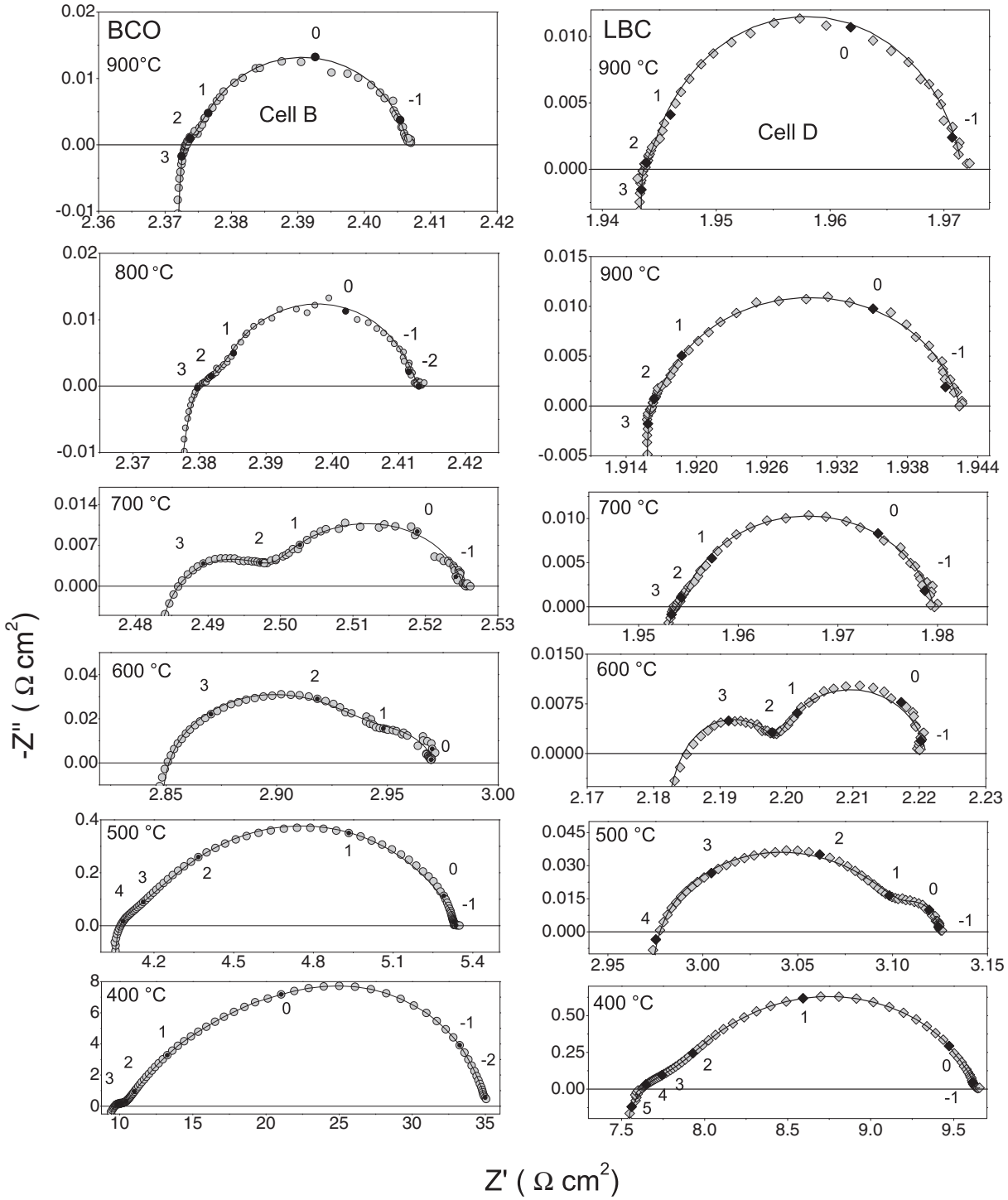

Figure 9. Variation of the impedance spectra with temperature ($400 \leq T \leq 900°C$) for the electrode $BaCoO_{3-\delta}$ in a cell type B and LBC with the cell configuration D. The solid line corresponds to the fit of the experimental data. The logarithm of the frequency is indicated in the Figure.

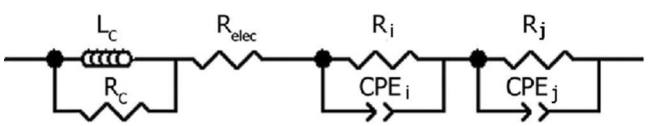

Figure 10. Equivalent circuit used for fitting impedance data. For $T > 550°C$, i = IF and j = LF while for $T < 550°C$ i = IF and j = HF or LF*.

to understand the process associated to each impedance arc we also carried out measurements as a function of pO_2 in the range $1 \times 10^{-3} < pO_2 < 1$ atm. Systematically, under pure oxygen, $pO_2 = 1$ atm, the impedance spectra consists only of one arc, which corresponds to the IF process as was observed previously.[6,20] As the pO_2 decreases the appearance of the LF process can be observed. In this case, both arcs increase in size although the LF contribution grows faster than the IF arc as the pO_2 decreases. Figures 13 and 14 show the variation of R_P, R_{LF} and R_{IF} as a function of pO_2 at $T = 600°C$ for $La_{0.3}Ba_{0.7}CoO_{3-\delta}$ and LBC electrodes, respectively. The other electrodes, BCO, BCFN,

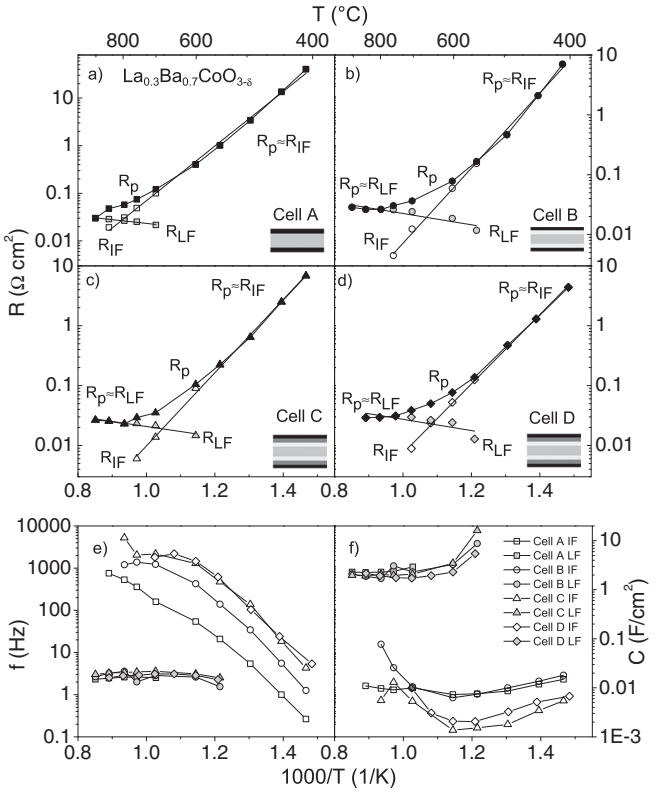

Figure 11. Arrhenius plots of the polarization resistances R_p, R_{IF} and R_{LF} obtained for electrodes prepared with $La_{0.3}Ba_{0.7}CoO_{3-\delta}$. Figures a-d correspond to cells A, B, C and D, respectively, while Figures 11e and 11f display the Arrhenius plots for the apex frequency and the capacitance, respectively, corresponding to the IF and LF contributions of the impedance spectra.

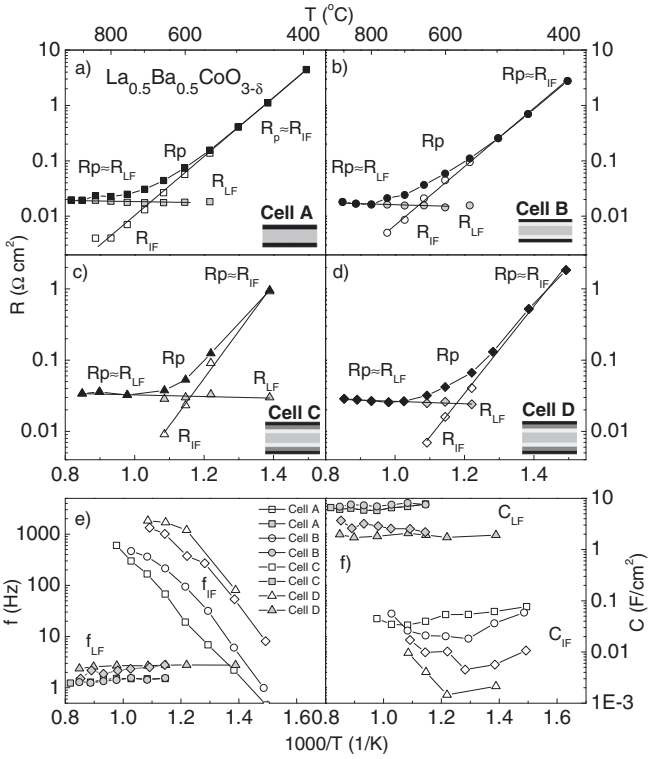

Figure 12. Arrhenius plots of the polarization resistances R_p, R_{IF} and R_{LF} obtained for electrodes prepared with $La_{0.5}Ba_{0.5}CoO_{3-\delta}$. Figures a-d correspond to cells A, B, C and D, respectively, while Figures 11e and 11f display the Arrhenius plots for the apex frequency and the capacitance, respectively, corresponding to the IF and LF contributions of the impedance spectra.

and BSCF, exhibit similar behavior. The variation of the polarization resistance with pO_2 is usually analyzed using the power law,

$$R = K \times (pO_2)^n \quad [1]$$

where *K* is a constant and the parameter *n* is related with the species involved in the electrode reaction and the process responsible of the electrode polarization[34–37] (see Table II).

Low frequency (LF) contribution.—The experimental data displayed in Figures 11 and 12 shows that the polarization resistance R_{LF} slightly increases with temperature and is practically independent of the material and electrode configuration. At T = 600°C the value of R_{LF} is in the range 0.02–0.04 Ω cm^2. The characteristic frequencies are in the range $1 \leq \nu_{LF} \leq 3$ Hz (Figures 11e and 12e), while the capacitance values are in the range $1.5 \leq C_{LF} \leq 8$ F/cm^2 as is shown in Figures 11f and 12f. Both ν_{LF} and C_{LF} show little variation with temperature. In regards to the effect of the pO_2 on R_{LF}, we listed in Table III the values of the parameter *n* obtained from the slope of the log (R_{LF}) vs. log (pO_2) curves, like those displayed in Figures 13 and 14, for the various electrode materials and cells. At T = 600°C we found that the parameter *n* for R_{LF} is systematically close to −1 regardless of the cell type. The value of the parameter *n*, the slight variation of R_{LF} with temperature and the magnitude of ν_{LF} and C_{LF} indicate R_{LF} can be associated to the oxygen gas diffusion through the electrode pores.[6,20,36,38–40]

Intermediate frequency (IF) contribution.—In regards to the IF contribution, experimental data displayed in Figures 11 and 12 show its dependence on temperature, cell configuration and, as we described in Optimization of the heat treatment temperature for the cathode preparation section, markedly on the temperature of the preparation heat-treatment. The polarization resistance R_{IF} decreases with increasing temperature indicating the contribution is thermally activated. The activation energies (E*a*) of R_{IF} calculated from the experimental data for the various electrode materials and cells are listed in Table IV. For LBC and BSCF the activation energy of R_{IF} increases ongoing from Cell A to cell D, although this trend was not confirmed by the other electrodes. In average, the lowest activation energy E*a* ∼0.84 (22) eV was obtained for BSCF, with variations from ∼0.6 eV for cell A to ∼1.0 eV for cells C and D. The low values of E*a* obtained for cells A and B are related to the presence of an extra contribution at low frequency and low temperature, described in a previous work and identified as LF*.[6] For cells C and D this process disappears resulting in E*a* values closer to those already reported for BSCF.[15,41–43] On the other hand, the highest value E*a* ∼ 1.4 eV corresponds to $BaCoO_{3-\delta}$, whose crystal structure is expected to be hexagonal in air at the temperature range of the impedance measurements. For LBC, $La_{0.3}Ba_{0.7}CoO_{3-\delta}$ and BCFN the activation energy average is in the range $1.1 \leq Ea \leq 1.18$ eV. These values are close to that reported by Amin et al.[44] for LBC, E*a* = 1.2 eV, but somewhat above the values reported by Pang et al.,[45] $0.87 \leq Ea \leq 1$ eV and Garces et al.,[46] $0.93 \leq Ea \leq 1.01$, also for LBC.

The lowest R_{IF} values were obtained, in general, for cells C and D corresponding to graded cathode electrodes. In contrast higher values were obtained, systematically, for cell A. The experimental data shows R_{IF} decreases with the electrode configuration following the order A > B > C > D. This behavior is related with the incorporation of a composite in cells C and D that helps reduce R_p[15,45,47] due to, for example, the extension of the ORR region into the porous electrode.[47] Finally, in these cells the pure cobaltite layer improves the current collection in comparison to the composite.[15,48] The apex frequency of the IF arc, displayed in Figures 11e and 12e for $La_{0.3}Ba_{0.7}CoO_{3-\delta}$ and LBC, respectively, increases with temperature from ∼ 0.1 Hz at 400–450°C to ∼10^2–10^3 Hz at 800–850°C indicating the relaxation time of this process is thermally activated. On the other hand,

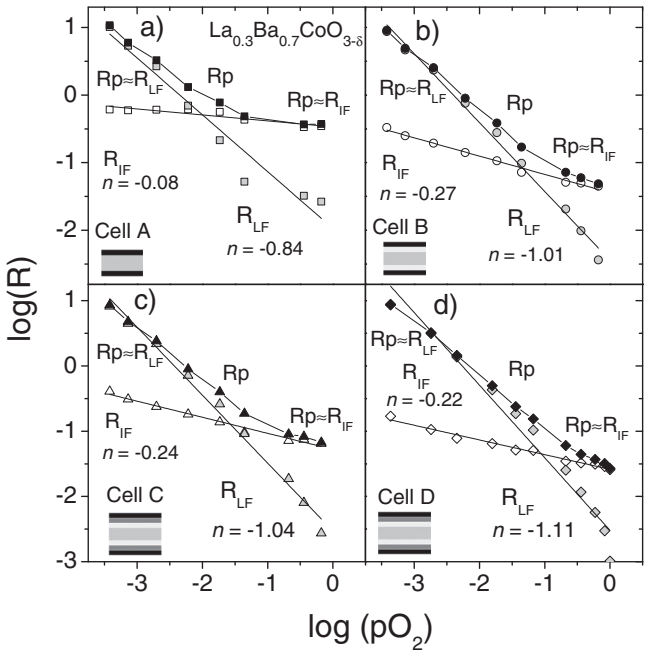

Figure 13. Variation of the polarization resistances R_p, R_{IF} and R_{LF} as a function of log (pO_2) at T = 600°C for cells A, B, C and D with electrodes prepared with $La_{0.3}Ba_{0.7}CoO_{3-\delta}$.

the range of variation of the capacitance, C_{IF}, is mostly between $\sim 1 \times 10^{-3}$ and ~ 0.1 F/cm^2, which are between 2 and 3 orders of magnitude lower than C_{LF} (see typical data in Figures 11f and 12f. As a function of temperature, C_{IF} shows no clear trend. In general, for a given compound cells C and D tend to exhibit lower capacitance values than cells A and B, although this order changes for BCFN. Additionally, we calculated the parameter *n* for R_{IF} from the log (R_{IF}) vs. log (pO_2) data at 600°C using Equation 1. The obtained values are

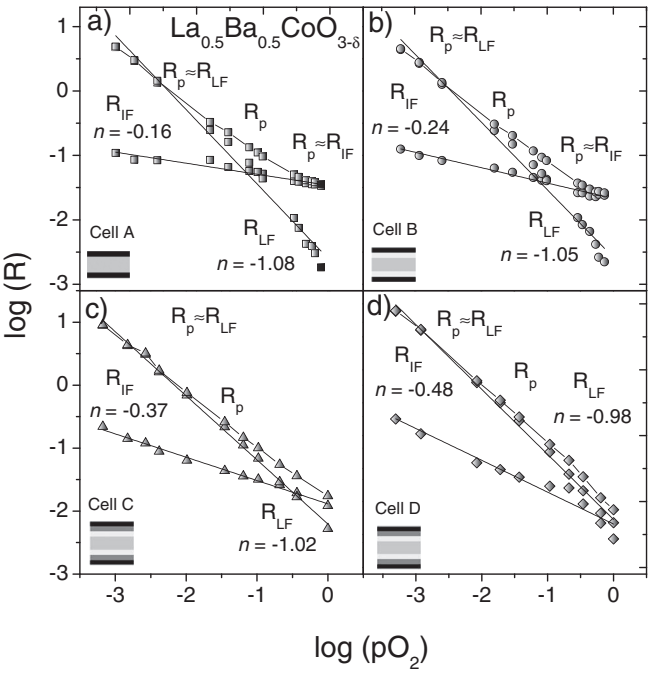

Figure 14. Variation of the polarization resistances R_p, R_{IF} and R_{LF} as a function of log (pO_2) at T = 600°C for cells A, B, C and D with electrodes prepared with $La_{0.5}Ba_{0.5}CoO_{3-\delta}$.

Table II. Polarization resistance process and its associated parameter *n* in Rp = K pO_2^n.

Rp contribution	*n*
$O_{ad}^- + e^- + V_O^{\bullet\bullet} \leftrightarrow O_o^x$	−0.25
$O_2 + 2e^- \leftrightarrow 2\,O_{ad}^-$	−0.5
$O_2 \leftrightarrow O_{2,ad}$	−1
O_2 gas diffusion	−1

listed in Table III. In this case for a given electrode material the parameter *n* changes with the cell type. This behavior is very clear for LBC, BCO and BSCF where *n* varies from ∼−0.1 to −0.5 as the electrode configuration is modified from cell A to cell D. This trend slightly changes for $La_{0.3}Ba_{0.7}CoO_{3-\delta}$since the parameter n varies from −0.08 to −0.25, while for BCFN it results close to −0.4 for cells A, B and C and then changes to −0.7 for cell D. As was detailed in Table II, a value of n ≈ −0.25 corresponds to the charge-transfer and reduction of the adsorbed atomic oxygen followed by the oxide ion incorporation into the electrode, n ≈ −0.5 is associated to the dissociation of molecular to atomic oxygen at the surface of the electrode, and n ≈ −1 to the adsorption of molecular oxygen to the surface electrode.[34,45,49] On the other hand, if the polarization resistance exhibits a negligible dependence with pO_2, the process is associated to the oxide ion transfer across the cathode/electrolyte interface.[45,50] Our experimental data indicates that for most of the electrode materials the parameter *n* for R_{IF} becomes more negative as the electrode arrangement includes layers containing GDC, which increases the surface area of the electrode but also the cobaltite/GDC interface. The value of n ∼ −0.1 obtained for most electrodes tested in cells A, suggest the process controlling R_{IF}, should be a mixture between the ion transfer at the electrode/electrolyte interface and the process of charge transfer taking place at the electrode surface and comprises the oxygen reduction and its incorporation to the lattice of the mixed conductor oxide.[50] Note that for cell A, the electrode-electrolyte interface is limited to the contact area between the electrode and the dense electrolyte. The incorporation of the GDC porous layer in cell B increases both the adherence and the contact area between the electrode and the electrolyte leading to a more negative value for parameter *n*, suggesting the limiting process for R_{IF} shifts toward the charge transfer at the electrode surface. This trend seems to increase in cells C and D where a composite layer of cobaltite+GDC was incorporated using GDC with increasing surface area. Thus, for these cells the exponent *n* shifts closer to −0.5 suggesting the dissociation of the oxygen molecule to atomic oxygen at the electrode surface followed by its incorporation into the electrode is the limiting process in all these cobaltites with high Ba content for cells C and D.

Conclusions

The electrochemical behavior of $La_{1-x}Ba_xCoO_{3-\delta}$ with x = 0.5, 0.7 and 1.0, BSCF and BCFN as cathode for IT-SOFC were studied. The phase relationship and formation of the cubic perovskite was controlled and monitored by XRD. The optimum temperature for electrode preparation was determined by impedance spectroscopy and was found between 900 and 950°C depending of the material. The lowest Rp values were obtained systematically for graded cathodes (cells C and D) formed by GDC/GDC+cobaltite/cobaltite. For instance, we obtained R_p = 0.036 and 0.039 Ω cm^2 at 600°C, in air, for $La_{0.5}Ba_{0.5}CoO_{3-\delta}$(cell D) and BSCF (cell C), respectively. The impedance spectra shows the presence of two processes taking place at intermediate (IF) and low frequency (LF). The LF process was associated to the O_2 gas diffusion through the electrode pores. Regarding the R_{IF} contribution, we found that the heat-treatment to attach the electrode to the electrolyte, mainly enhance the kinetic of those processes related to R_{IF}. This process, that is dominant at T≤ 700°C, exhibits activation energy average values in the range 0.84 ≤ E*a* ≤ 1.4 eV. The minimum was found for BSCF, E*a* = 0.84 eV, while the highest value, E*a* = 1.4 eV, corresponds to $BaCoO_{3-\delta}$. For LBC, $La_{0.3}Ba_{0.7}CoO_{3-\delta}$

Table III. Parameter *n* values with their statistical errors for R_{LF} and R_{IF} at T = 600°C for the various electrodes configurations.

	LBC		$La_{0.3}Ba_{0.7}CoO_{3-\delta}$		BCO		BCFN		BSCF	
	R_{LF}	R_{IF}	R_{LF}	R_{IF}	R_{LF}	R_{IF}	R_{LF}	R_{IF}	R_{LF}	R_{IF}
Cell A	−1.08 (4)	−0.16 (1)	−0.84 (7)	−0.08 (2)	−1.24 (3)	−0.20 (3)	−1.01 (3)	−0.45 (2)	−1.17 (8)	−0.07 (2)
Cell B	−1.05 (4)	−0.23 (1)	−1.01 (3)	−0.27 (1)	−0.91 (4)	−0.35 (3)	−1.02 (3)	−0.38 (2)	−0.97 (4)	−0.10 (2)
Cell C	−1.01 (2)	−0.37 (1)	−1.04 (4)	−0.24 (1)	−0.93 (6)	−0.43 (4)	−0.81 (3)	−0.48 (2)	−1.06 (3)	−0.30 (1)
Cell D	−0.98 (2)	−0.48 (4)	−1.11 (8)	−0.22 (1)	−0.73 (4)	−0.51 (2)	−0.97 (2)	−0.67 (4)	−0.97 (3)	−0.42 (2)

Table IV. Activation energies values in eV with their statistical errors obtained for the polarization resistance associated to the intermediate frequency contribution R_{IF} in air.

	LBC	$La_{0.3}Ba_{0.7}CoO_{3-\delta}$	BCO	BCFN	BSCF
Cell A	1.05 (2)	1.13 (2)	1.41 (2)	1.00 (1)	0.58 (5)
Cell B	1.05 (2)	1.24 (3)	1.33 (2)	1.15 (6)	0.72 (6)
Cell C	1.31 (6)	1.21 (2)	1.16 (3)	1.02 (3)	1.04 (4)
Cell D	1.21 (4)	1.14 (2)	1.58 (12)	1.21 (5)	1.01 (2)
Average	1.15 (15)	1.18 (5)	1.40 (20)	1.10 (10)	0.84 (22)

and BCFN, E*a* take values between 1.1 and 1.18 eV. The parameter *n* obtained from the $\log(R_{IF})$ vs $\log(pO_2)$ plots tends to vary from ~ -0.1 to -0.5 following the order A > B > C > D. This suggests the rate-limiting process changes with the electrode configuration from a mixture of ion transfer at the electrode/electrolyte interface and the charge transfer at the electrode surface to a mixture between this last process and the dissociation of the oxygen molecule followed by the incorporation of the oxide ion into the electrode.

Acknowledgments

The authors thank L. Prado for English revision of the manuscript. This work was supported by Comisión Nacional de Energía Atómica (CNEA), Consejo Nacional de Investigaciones Científicas y Técnicas (CONICET) and Agencia Nacional de Promoción Científica y Técnica (ANPCyT), Argentina, through PIP 112 2013 0100513 CO, and PICT 2013-1032, respectively.

References

1. Z. Gao, L. Mogni, E. Miller, J. Railsback, and S. Barnett, *Energy Environ. Sci.*, **9**, 1602 (2016).
2. Y. Teraoka, H. M. Zhang, S. Furukawa, and N. Yamazoe, *Chem. Lett.*, 1743 (1985).
3. Y. Teraoka, H. M. Zhang, K. Okamoto, and N. Yamazoe, *Mat. Res. Bull.*, **23**, 51 (1988).
4. Z. Shao and S. M. Haile, *Nature*, **431**, 170 (2004).
5. W Zhou, R Ran, and Z Shao, *J. Power Sources.*, **192**, 231 (2009).
6. C. Setevich, F. Prado, and A. Caneiro, *J Solid State Electrochem*, **20**, 1633 (2016).
7. C. Zhu, X. Liu, C. Yi, L. Pei, D. Yan, J. Niu, D. Wang, and W. Su, *Electrochem. Commun.*, **11**, 958 (2009).
8. A. Tarancon, S. Skinner, R. Chater, H. Hernández-Ramírez, and J. Kilner, *J. Mater. Chem.*, **17**, 3175 (2007).
9. J.-H. Kim and A. Manthiram, *J. Electrochem. Soc.*, **155**, B385 (2008).
10. R. Shannon, *Acta Cryst*, **A32**, 751 (1976).
11. R. Merkle, Y. Mastrikov, E. Kotomin, M. Kuklja, and J. Maier, *J. Electrochem. Soc.*, **159**, B219 (2012).
12. T. Ishihara, S. Fukui, H. Nishiguchi, and Y. Takita, *Solid State Ionics*, **152–153**, 609 (2002).
13. T. Ishihara, S. Fukui, H. Nishiguchi, and Y. Takita, *J. Electrochem. Soc.*, **149**, A823 (2002).
14. C. Setevich, L. Mogni, F. Prado, and A. Caneiro, *J. Electrochem. Soc.*, **159**, B72 (2012).
15. C. Setevich, L. Mogni, F. Prado, and A. Caneiro, *Int. J. Hydrogen Energy*, **37**, 14895 (2012).
16. G. Rupp, A. Schmid, A. Nenning, and J. Fleig, *J. Electrochem. Soc.*, **163**, F564 (2016).
17. S. Švarcová, K. Wiik, J. Tolchard, H. J. M. Bouwmeester, and Tor Grande, *Solid State Ionics*, **178**, 1787 (2008).
18. C. Zhu, X. Liu, C. Yi, L. Pei, D. Yan, J. Niu, D. Wang, and W. Su, *Electrochem. Commun.*, **11**, 958 (2009).
19. Y. Cheng, H. Zhao, D. Teng, F. Li, X. Lu, and W. Ding, *J. Membr. Sci.*, **322**, 484 (2008).
20. C. Setevich, F. Prado, D. Florio, and A. Caneiro, *J. Power Sources.*, **247**, 264 (2014).
21. C. Setevich, L. Toscani, S. Larrondo, F. Prado, and A. Caneiro, *Solid State Ionics*, **300**, 140 (2017).
22. J. Xie, Y. Ju, T. Sakai, and T. Ishihara, *J. Solid State Electrochem.*, **17**, 2251 (2013).
23. H. Gu, H. Chen, L. Gao, and L. Guo, *Electrochimica Acta*, **54**, 7094 (2009).
24. T. Jiang, Z. Wang, B. Ren, J. Qiao, W. Sun, and K. Sun, *J. Power Sources*, **247**, 858 (2014).
25. B. Wei, Z. Lü, W. Jiang, X. Zhu, and W. Su, *Electrochimica Acta*, **134**, 136 (2014).
26. Y. Xia, T. Armstrong, F. Prado, and A. Manthiram, *Solid State Ionics*, **149**, 11 (2000).
27. J. Rodríguez-Carvajal, Fullprof: a program for Rietveld Refinement and Profile Matching Analysis of Complex Powder Diffraction Patterns, Laboratoire Léon Brillouin (CEA-CNRS).
28. Zview version 2.0b copyright 1990–2005, *Scribner Associates*, Inc. D. Johnson.
29. K. Yamaura and R. Cava, *Solid State Commun*, **115**, 301 (2000).
30. A. J. Jacobson and J. L. Hutchison, *J. Solid State Chem.*, **35**, 334 (1980).
31. S. W. Strauss, I. Fankuchen, and R. Ward, *J. Am. Chem. Soc.*, **73**, 5084 (1951).
32. H. Yung, L. Jian, and S. Jiang, *J. Electrochem Soc.*, **159**, F794 (2012).
33. K. Wang, R. Ran, W. Zhou, H. Gu, Z. Shao, and J. Ahn, *J. Power Sources*, **179**, 60 (2008).
34. Y. Takeda, R. Kanno, M. Noda, Y. Tomoda, and O. Yamamoto, *J. Electrochem Soc.*, **134**, 2656 (1987).
35. A. Ringuedé and J. Fouletier, *Solid State Ionics*, **139**, 167 (2001).
36. C. Deportes, M. Duclot, P. Fabry, J. Fouletier, A. Hammou, M. Kleitz, E. Siebert, and J. L. Souquet, *Electrochimie des Solides*, Presses Universitaires de Grenoble. Grenoble 1994.
37. C.-Y. Yoo, D. S. Yun, S.-Y. Park, J. Park, J. H. Joo, H. Park, M. Kwak, and J. H. Yu, *Electrocatalysis*, **7**, 280 (2016).
38. N. Grunbaum, L. Dessemond, J. Fouletier, F. Prado, L. Mogni, and A. Caneiro, *Solid State Ionics*, **180**, 1448 (2009).
39. L. Mogni, N. Grunbaum, F. Prado, and A. Caneiro, *J. Electrochem. Soc.*, **158**, B202 (2011).
40. S. B. Adler, *Chem. Rev.*, **104**, 4791 (2004).
41. W. Zhou, R. Ran, Z. Shao, W. Zhuang, J. Jia, H. Gu, W. Jin, and N. Xu, *Acta Materialia*, **56**, 2687 (2008).
42. B. Liu, Y. Zhang, and L. Zhang, *Int. J. Hydrogen Energy*, **34**, 1008 (2009).
43. Z. Chen, R. Ran, W. Zhou, Z. Shao, and S. Liu, *Electrochimica Acta*, **52**, 7343 (2007).
44. R. Amin and K. Karan, *J. Electrochem. Soc.*, **157**, B285 (2010).
45. S. Pang, X. Jiang, X. Li, Q. Wang, and Z. Su, *Int. J. Hydrogen Energy*, **37**, 2157 (2012).
46. D. Garces, A. Soldati, H. Troiani, A. Montenegro-Hernández, A. Caneiro, and L. Mogni, *Electrochimica Acta*, **215**, 637 (2016).
47. E. Murray, M. Sever, and A. Barnett, *Solid State Ionics*, **148**, 27 (2002).
48. Y. Guo, Y. Zhou, D. Chen, H. Shi, R. Ran, and Z. Shao, *J. Power Sources*, **196**, 5511 (2011).
49. D. Chen, R. Ran, K. Zhang, J. Wang, and Z. Shao, *J. Power Sources*, **188**, 96 (2009).
50. M. J. Escudero, A. Aguadero, J. A. Alonso, and L. Daza, *J. Electroanalytical Chem.*, **611**, 107 (2007).